Bulk and surface electronic structures of the semimetal Bi studied by angle-resolved photoemission spectroscopy

Akinori Tanaka, Masayuki Hatano, Kazutoshi Takahashi, Hiroyuki Sasaki, Shoji Suzuki, and Shigeru Sato
Department of Physics, Graduate School of Science, Tohoku University, Aoba-ku, Sendai 980-8578, Japan
(Received 22 May 1998)

An angle-resolved photoemission study of the Bi (111) single crystal has been carried out in order to investigate in detail the bulk and surface electronic structures. The valence-band photoemission spectra of the Bi (111) single crystal exhibit the features derived from the Bi $6p$-derived bulk valence band, the surface state in the spin-orbit gap, and the surface resonance state. From the detailed angle-resolved photoemission spectra, the dispersion relations of the bulk valence band of Bi were determined along the T-U high-symmetry line in the bulk Brillouin zone. These experimental band dispersions are compared with the theoretical results of the band calculations, obtained by a pseudopotential method and a recent third-neighbor tight-binding method. The dispersion relation of the surface state in the spin-orbit gap and surface resonance state on the Bi (111) clean surface were also determined experimentally along the $\bar{\Gamma}$-$\bar{M}$ symmetry line in the surface Brillouin zone. [S0163-1829(99)11703-X]

I. INTRODUCTION

The physical properties of semimetal Bi, as well as the other group-V semimetals, have attracted much interest of many investigators for a long time. Bulk Bi single crystal has a rhombohedral ($A7$) crystal structure with two atoms per unit cell, which is distorted face-centered-cubic lattice along the (111) direction.[1] This distortion yields a rather complicated electronic structure. For example, bulk Bi exhibits a weak overlap between the valence and conduction bands, which leads to a small number of free electrons and holes. It has also small indirect energy gap in the vicinity of the Fermi level.[2] Connected with this peculiar electronic structure, bulk Bi shows small effective masses along certain axes, high-carrier mobility, and a long mean-free path.[2] Moreover, quantum size effects in semimetallic nanostructures recently have attracted much interest. In a semimetallic nanofilm, the confinement of carriers (electrons and holes) in the direction normal to the nanofilm leads to quantized electronic states of both carriers as a function of the nanofilm thickness. On decreasing the semimetallic nanofilm thickness, the semimetal-to-semiconductor transition should occur when the energy shift due to quantum size effects become large enough to raise the lowest quantized two-dimensional electron subband to an energy higher than that of the uppermost quantized two-dimensional hole subband. Bismuth is considered to be an ideal material for the study of the quantum confinement effects in semimetallic systems, since it has a small effective mass and long mean-free path as described above, so that the energy shifts due to quantum confinement effects may be remarkable in Bi nanofilms. In order to elucidate these quantum size effects on the semimetallic Bi nanofilms, it is indispensable to understand the bulk electronic structure of parental bulk Bi single crystal. However, most of the experimental[3–6] and theoretical[7–12] studies for bulk Bi have been carried out in order to investigate the carriers (electrons and holes) themselves and the shapes of the electron and hole Fermi surfaces. In contrast to an understanding of the features near the Fermi surfaces, reports of the overall electronic band structures, such as the photoemission studies, are very few to date for the bulk Bi single crystal.

In this work, we carried out an angle-resolved photoemission study of Bi (111) single crystals epitaxially grown on Si (111) substrates so as to elucidate the bulk electronic structures of semimetal Bi. Angle-resolved photoemission spectroscopy has been used to determine the electronic structures directly, however, to our knowledge there is only one recent report of an angle-resolved photoemission study by Jezequel, Thomas, and Pollini[13] to date that highlights the bulk electronic structures of semimetal Bi. In order to understand the overall electronic band structure in detail, it is necessary to observe the electronic band structure along the various high-symmetry lines in the Brillouin zone (BZ) with better energy and angular resolution. In addition, spin-orbit coupling is large in bulk Bi single crystal as is well known, and the existence of a surface state in the spin-orbit energy gap has been reported.[14,15] In this paper, we report the results of the angle-resolved photoemission measurements at low temperature for bulk Bi (111) epitaxial crystallites employing a better energy resolution of about 40 meV and angular resolution of about $\pm 0.4°$. From these results and comparison with the theoretical results of the band calculations, we discuss the bulk and surface electronic structures of bulk Bi in detail.

II. EXPERIMENT

Bulk Bi single crystals used in our experiment were grown by molecular-beam epitaxy (MBE) using a JPS-100 (ANELVA Co. Ltd.) MBE system connected directly to a ARUPS 10 (VG Scientific Co. Ltd.) photoelectron spectrometer. The base pressure of the MBE system was in the 10^{-9} Pa range. The substrates used in the epitaxial growth were Si (111) single crystals. After a chemical treatment by the method of Ishizaka and Shiraki,[16] Si (111) single-crystalline

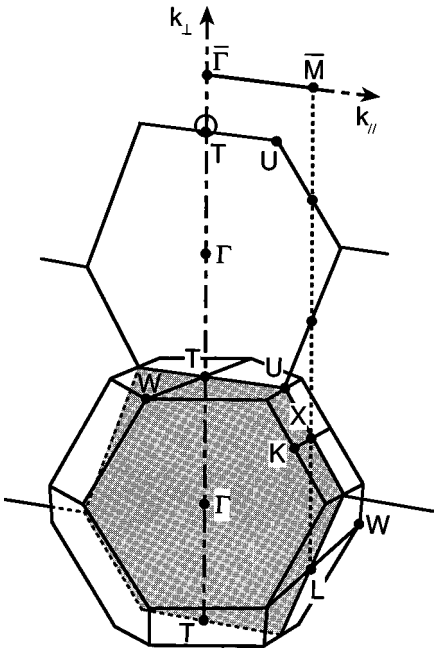

FIG. 1. Bulk Brillouin zone of the rhombohedral structure with high-symmetry points and extended zone scheme of the Γ-L-X plane. High-symmetry line along the $\bar{\Gamma}$-$\bar{M}$ direction in the surface Brillouin zone are also indicated. Open circle represent the corresponding free-electron-like final state with He I resonance line ($h\nu=21.2$ eV).

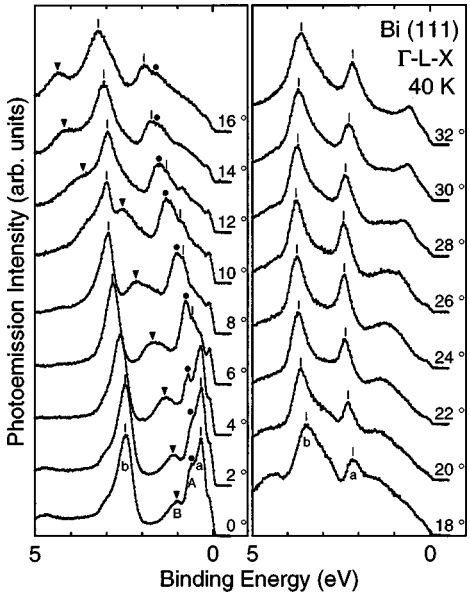

FIG. 2. Angle-resolved valence-band photoemission spectra at various photoelectron emission angle in the Γ-L-X plane of the bulk Brillouin zone for the Bi (111) epitaxial film with a thickness of 150 nm excited by the He I resonance line ($h\nu=21.2$ eV) at 40 K. Solid circles (peak A), solid triangles (peak B), and bars (peaks a and b) represent the main photoemission peaks. The polar emission angles with respect to the surface normal are indicated for each spectrum.

wafers were introduced to the growth chamber of MBE system. The substrates were annealed around 850 °C to obtain the clean surface prior to epitaxial growth of Bi. The Bi epitaxial films were deposited by the Knudsen cell onto Si (111) substrates at room temperature. The deposition rates for Bi were about 0.01 nm/sec as determined by a quartz thickness monitor. In this work, we carried out angle-resolved photoemission measurements on the samples with a thickness of 150 nm. The cleanliness and structure of the sample were checked by Auger electron spectroscopy, x-ray photoemission spectroscopy, and low-energy electron diffraction (LEED) patterns. By the above method, we observed a clear sixfold LEED pattern, indicating a rhombohedral (111) crystallite, and succeeded in getting the Bi (111) epitaxial films identical with the bulk Bi single crystal.

The thus-prepared samples were transferred into the photoelectron spectrometer through the ultrahigh vacuum chamber without exposure to air. Angle-resolved photoemission measurements were performed with the He I resonance line ($h\nu=21.2$ eV) as the excitation source. The base pressure of the photoelectron spectrometer was also in the 10^{-9} Pa range. Total energy resolution for the measurement excited by He I resonance radiation ($h\nu=21.2$ eV) was about 40 meV, and the angular resolution was about $\pm 0.4°$. From the orientation of the observed LEED pattern, we decided on the photoelectron detection planes for the angle-resolved photoemission measurements. Figure 1 shows a bulk Brillouin zone of the rhombohedral structure with high-symmetry points. The measurements in the present work were carried out in the photoelectron detection plane with the high-symmetry line in the bulk BZ: Γ-T-U-L-U-X-U-T-Γ (abbreviated to Γ-L-X) plane. All photoemission measurements reported here were recorded at low temperature (40 K) using a He refrigerator in order to minimize the phonon-assisted contributions to the photoemission spectra, since the bulk Bi single crystal has a low-Debye temperature of 120 K.[14,17] The photoemission spectra showed no change in the course of the measurements. The Fermi level of the sample was determined by comparison with a gold film deposited on the sample surface.

III. RESULTS AND DISCUSSION

Figure 2 shows angle-resolved valence-band photoemission spectra at various photoelectron emission angles, measured at 40 K for Bi (111) epitaxial film with a thickness of 150 nm excited by He I ($h\nu=21.2$ eV). This photoelectron detection plane corresponds to the Γ-L-X plane in the bulk BZ and also the $\bar{\Gamma}$-$\bar{M}$ symmetry line in the surface Brilluoin zone (SBZ). The present angle-resolved photoemission spectrum with a normal emission geometry of $\theta=0°$ (the normal emission spectrum) is identical with the previously reported ones for the bulk single-crystalline Bi (111) clean surface.[13–15] This indicates that the electronic structure of our present Bi (111) epitaxial film with a thickness of 150 nm is identical with those of the bulk single-crystalline Bi (111) clean surface. Therefore, this thickness is large enough that quantum confinement effects may be ignored. As shown in Fig. 2, the normal emission spectrum of Bi (111) epitaxial crystallite shows sharp structures with the higher intensities around 0.3 and 2.5 eV binding energy (peaks a and b). From the previous results of the photon-energy-dependent photoemission studies with synchrotron radiation[13,14] and the ''crud'' test (Ar adsorption and Ar ion sputtering) for the Bi

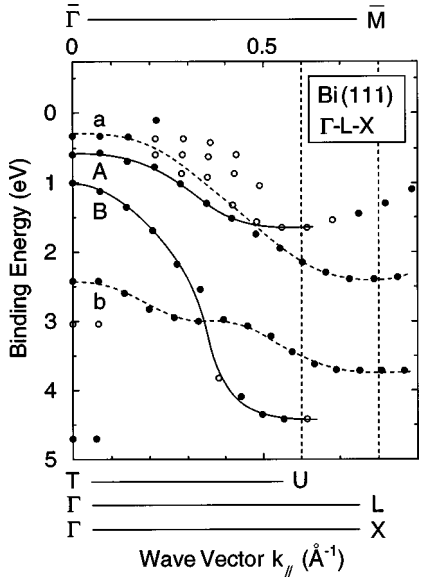

FIG. 3. Experimental energy dispersion for Bi (111) in the Γ-L-X plane of the bulk Brillouin zone. Wave vectors parallel to the surface corresponding the high-symmetry lines along the T-U, Γ-L, and Γ-X directions in the bulk Brillouin zone and along the $\bar{\Gamma}$-$\bar{M}$ direction in the surface Brillouin zone are also given. Solid and open circles represent prominent and weak structures in the valence-band photoemission spectra, respectively. Solid and dashed lines are drawn to guide the eye for the energy dispersion of the Bi $6p$-derived bulk valence-band states (peaks A and B in Fig. 2) and the surface-derived states (peaks a and b in Fig. 2), respectively.

(111) clean surface,[14,15] these structures originate in surface-derived electronic states on the Bi (111) clean surface. From a comparison with previous angle-resolved photoemission study obtained in normal emission with a tunable synchrotron radiation,[13] the observed structure around 0.3 eV corresponds to the surface state in the spin-orbit gap at the $\bar{\Gamma}$-symmetry point of the SBZ, while that around 2.5 eV corresponds to the surface resonance state, which is not be located in the energy gaps and hybridizes with the bulk electronic states. This observation for the present Bi (111) epitaxial film confirms again the existence of both the surface state in the spin-orbit gap and the surface resonance state on the Bi (111) clean surface as determined in previous studies.[14,15] In addition to the surface-derived electronic states as described above, the normal emission spectrum exhibits small structures. It is considered that these structures originate from Bi $6p$-derived bulk valence-band states.

As shown in Fig. 2, it is found that the binding energies of the bulk and surface-derived electronic states observed in the normal emission spectrum change as a function of photoelectron emission angle. This means that these electronic states have an energy dispersion along the direction parallel to the sample surface. In order to clarify the dispersion relation of each structure in the valence-band photoemission spectrum, we plot the binding energies of these electronic states versus the wave vector parallel to the sample surface in Fig. 3. In Fig. 3, the dashed lines are drawn to guide the eye for the energy dispersion relations of the surface-derived electronic states (surface state in the spin-orbit gap and the surface resonance state, as assigned above) and the other points correspond to the Bi $6p$-derived bulk valence-band states. First, we discuss the Bi $6p$-derived bulk valence-band states. The solid lines are drawn to guide the eye for the energy bulk valence-band states. The solid lines are drawn to guide the eye for the energy dispersion relation of the prominent Bi $6p$-derived bulk valence-band states (peaks A and B in Fig. 2) which we can trace by increasing the photoelectron emission angle to the region around the zone boundary. These bulk electronic features denoted by the solid lines will be discussed below. In the photoemission process, photoelectron momentum broadening in the direction normal to the sample surface, which produces a small ambiguity in the initial states along the direction normal to the sample surface, takes place.[18] This causes the initial states with a high density of states, such as electronic states at high-symmetry points, to appear as the distinct structures in the photoemission spectra, and electronic state originating from several high-symmetry lines to be often observed only due to the conservation of the wave vector parallel to the sample surface.[19] Compared with the bulk BZ for the rhombohedral structure (see Fig. 1), the present photoelectron Γ-L-X detection plane includes the high-symmetry line along the T-U, Γ-L, and Γ-X directions. Due to electron momentum broadening as described above, there is a possibility that electronic states originating from the high-symmetry lines along the T-U, Γ-L, and Γ-X directions in the bulk BZ are observed in the angle-resolved photoemission spectra detected in the Γ-L-X plane. The corresponding wave vector parallel to the sample surface of each high-symmetry line is also given in Fig. 3. As shown in Fig. 3, both electronic states traced by the solid lines exhibit a relatively flat dispersion around the wave vector corresponding to the U high-symmetry point of the bulk BZ. This indicates that these observed electronic states have a high density of states at the U high-symmetry point of the bulk BZ. Therefore, it is concluded that these observed energy dispersion, denoted by the solid lines in Fig. 3, originate in the dispersion of the Bi $6p$-derived valence-band states along the T-U high-symmetry line in the bulk BZ. The additional structures observed near the Fermi level (which is not traced by the solid line in Fig. 3) may also originate in the dispersion along the T-U high-symmetry line, which contributes to the hole pocket at the T high-symmetry point. However, the degree of the electron momentum broadening normal to the sample surface depends on the material (electronic band structure, etc.) and the experimental conditions (exciting photon energy, photoelectron detection angle, etc.). The other interpretation in terms of direct $k_{\perp}$-conserving transitions has also been adopted successfully for the interpretation of the angle-resolved photoemission for a number of metals and semiconductors. In the normal emission geometry of the present work, electronic states in the (111) direction (from Γ to T in reciprocal space) of the bulk BZ are sampled (see Fig. 1). The difference in the electron wave vector between the initial and final states for the photoexciting process is 2.36 A^{-1} at the photon energy of $h\nu = 21.2$ eV. The reciprocal lattice vector $\mathbf{G}$ in the Γ-T-Γ direction is 1.547 A^{-1}. This leads to $k_{\perp} = |2.36\ A^{-1} - nG| = 0.814\ A^{-1}$ for a photon energy of $h\nu = 21.2$ eV.[15] The corresponding free-electron-like final state excited with He I resonance line is represented by the open circle through the extended zone scheme in Fig. 1. As shown in Fig. 1, the photoemission spectrum at the normal

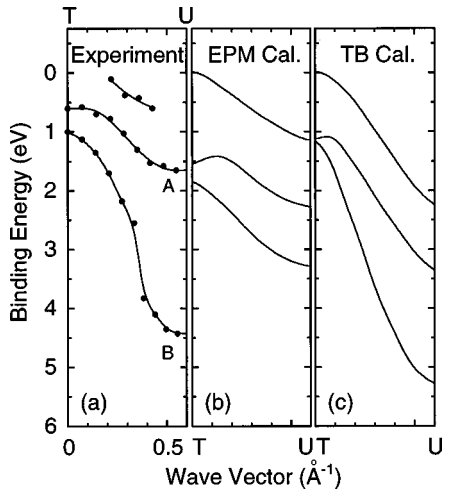

FIG. 4. Experimental and theoretical valence-band dispersion along the T-U high-symmetry line in the bulk Brillouin zone for bulk Bi. (a) Experimental valence-band dispersion along the T-U high-symmetry line as shown in Fig. 2. Solid lines are drawn to guide the eye for the energy dispersions. (b) Theoretical valence-band dispersion along the T-U high-symmetry line by means of the empirical pseudopotential method by Golin. (c) Theoretical valence-band dispersion along the T-U high-symmetry line obtained by means of a third-neighbor empirical tight-binding method by Liu *et al.*

emission geometry using a He I radiation for Bi (111) single crystal investigates the electronic states near the T high-symmetry point of the bulk BZ, and angle-resolved photoemission spectra at various emission angles in the present photoelectron detection plane with the He I radiation may trace the T-U high-symmetry line in the bulk BZ. It is considered that this is consistent with the fact that band dispersions originating from the T-U high-symmetry line are dominantly observed for the wide wave-vector region as shown in Fig. 3. Incidentally, the structures observed around 3 and 4.5 eV binding energies at small photoelectron emission angles may originate in the electronic states around the Γ high-symmetry point due to electron momentum broadening. Hence, we will discuss in particular the bulk valence-band structure around the T-U high-symmetry line below.

As shown in Fig. 3, it is found that the binding energies at the T high-symmetry point are 0.6 and 1.0 eV and those at the U high-symmetry point are 1.7 and 4.4 eV. It is also found that the bandwidths of the second and third Bi $6p$-derived valence bands along the T-U high-symmetry line (peaks A and B) are about 1.1 and 3.4 eV, respectively. In order to study these experimental energy dispersions of the bulk Bi single crystal in more detail, we compared them with the theoretical results of band calculations by means of an empirical pseudopotential model (EPM) method by Golin[10] and a recent third-neighbor empirical tight-binding (TB) method by Liu *et al.*[12] Figure 4 shows the experimental valence-band dispersions along the T-U high-symmetry line of bulk Bi single crystals, together with the theoretical dispersion curves obtained by Golin[10] and by Liu *et al.*[12] In the EPM band calculation by Golin, the pseudopotential is formed by a few adjustable parameters in order to reproduce the experimental results, and consists of three distinct terms: V_{loc}, a local potential that is the dominant term; V_s, an l-dependent term; and V_{so}, a term representing the spin-orbit coupling. This EPM band calculation also includes a spin-orbit coupling parameter λ. It successfully reproduces the effective mass anisotropies and optical data, but the magnitude of the effective masses differs from experimental data by a factor of 3. On the other hand, the third-neighbor empirical TB band calculation by Liu *et al.* includes spin-orbit coupling and third-neighbor interactions, and has 14 adjustable parameters: E_s, E_p, $V_{ss\sigma}$, $V_{sp\sigma}$, $V_{pp\sigma}$, $V_{pp\pi}$, $V'_{ss\sigma}$, $V'_{sp\sigma}$, $V'_{pp\sigma}$, $V'_{pp\pi}$, $V''_{ss\sigma}$, $V''_{sp\sigma}$, $V''_{pp\sigma}$, and $V''_{pp\pi}$. Here, E_s and E_p are the on-site s- and p-orbital energies, respectively. The unprimed, primed, and double-primed parameters are the nearest-neighbor, next-nearest neighbor, and third-neighbor interaction parameters. This TB band calculation successfully reproduces the small overlap of valence and conduction bands, the electron and hole effective masses, and the shapes of the electron and hole Fermi surfaces. From a comparison of our experimental valence-band dispersions with the EPM band calculation as shown in Figs. 4(a) and 4(b), it seems that the calculation reproduces the qualitative tendency of each band dispersion. Since it also reproduces the features near the Fermi level, the first Bi $6p$-derived band is reproduces relatively well. However, a large quantitative difference in both binding energy and bandwidth of the second and third Bi $6p$-derived valence bands is found. In order to improve the agreement in both binding energy and bandwidth between the experimental results and this EPM band calculations, it is considered necessary to modify the term V_{loc}, the term V_{so}, and the spin-orbit coupling parameter λ in particular. That is, by adjusting the term V_{loc}, the bandwidths may be increased, so that by adjusting the term V_{so} and the spin-orbit parameter λ, one may spread and shift the second and third Bi $6p$-derived band in our spectra, and lower the lowest Bi $6p$-derived band, leading to the improvement of the agreement with the experimental dispersions. Jezequel, Thomas, and Pollini also compared their experimental dispersion along the Γ-T high-symmetry line with this band calculation.[13] However, Jezequel, Thomas, and Pollini observed only one structure around 0.3 eV binding energy, originating from the surface states (peak A in Ref. 13), and discussed about only one Bi $6p$-derived band (peak B in Ref. 13) corresponding to our present third Bi $6p$-derived band. On the other hand, we distinguish three structures around 0.3 eV and observe the first and second Bi $6p$-derived band as described above. Therefore, we have expanded the discussions about all Bi $6p$-derived bands along the T-U high-symmetry line in the present work, and confirm again that this EPM band calculation fails to quantitatively reproduce the experimental dispersion of all Bi $6p$-derived bands. As shown in Figs. 4(a) and 4(c), it is found that the TB band calculations by Liu *et al.* also reproduces the qualitative tendency of each experimental band dispersion. In addition, the agreement with the present experimental valence-band dispersions seems improved compared with the EPM calculation. Especially, the agreement of the bandwidth of each Bi $6p$-derived valence band improves in this TB calculation. However, a quantitative difference in both binding energy and bandwidth is found as before. It also seems that the agreement with the

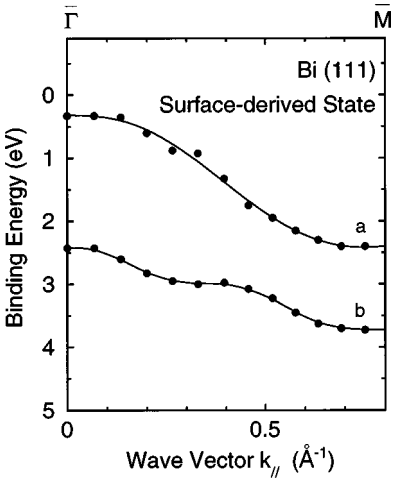

FIG. 5. Energy dispersions of the surface-derived electronic states (peaks *a* and *b* in Fig. 2) along the $\bar{\Gamma}$-$\bar{M}$-symmetry line of the surface Brillouin zone for the clean Bi (111) surface. The solid lines are drawn to guide the eye for the energy dispersions of the surface-derived states. The observed energy dispersions with lower and higher binding energies correspond to the surface state in a spin-orbit gap (at the $\bar{\Gamma}$ point of the surface Brillouin zone) and the surface resonance state, respectively.

experimental dispersionfor the second Bi 6*p*-derived valence band is worse. These results indicate that it is also necessary to modify the TB parameters and the spin-orbit parameter λ even for the TB band calculation in order to reproduce well the present experimental dispersions. Both band calculations have been carried out in order to fit the bands to the detailed experimental data in the vicinity of the Fermi level, such as band overlaps, effective masses of electrons and holes, shape of the Fermi surface at the electron and hole pockets, and small indirect gap, instead of considering the overall valence-band structure. Therefore, in order to fully discuss the experimental valence-band dispersions, a new *ab initio* band calculation, which pays attention to the overall valence-band structure would be necessary.

The next step in the present work is to discuss the surface-derived electronic strucutres (peaks *a* and *b*), denoted by the dashed lines in Fig. 3. As described above, the observed surface-derived electronic states with the lower and higher binding energies originate in the surface state in the spin-orbit gap and the surface resonance state, respectively. As shown in Fig. 3, it is clear that the dispersion relations of these surface-derived electronic states are symmetric with respect to the $\bar{M}$ symmetry point of the SBZ, indicating that these surface-derived states have a periodicity with the $\bar{\Gamma}$-$\bar{M}$ wave vector on the SBZ. In order to clarify the dispersion relation of these surface-derived states on the Bi (111) clean surface, we replot the binding energies of these surface-derived states versus the wave vector parallel to the sample surface along the $\bar{\Gamma}$-$\bar{M}$ symmetry line of the SBZ in Fig. 5. As shown in Fig. 5, it is clear that both surface state and surface resonance on Bi (111) have an energy dispersion along the $\bar{\Gamma}$-$\bar{M}$ symmetry line of the SBZ and the dispersion relation of these surface-derived electronic states were definitely determined in the SBZ. These dispersion relations are indicated by the solid lines in Fig. 5. It is found that the energy dispersion of the surface state in the spin-orbit gap (at the $\bar{\Gamma}$-symmetry point) along the $\bar{\Gamma}$-$\bar{M}$ symmetry line of SBZ is on the order of 2 eV and that this dispersion relation is almost the same as that along the $\bar{\Gamma}$-*K*-symmetry line of the SBZ obtained in previous work.[14,15] An important point to note is that this surface state dispersion, denoted by the dashed line in Fig. 3, intersects the bulk Bi 6*p*-derived valence band, denoted by the solid line, at a finite wave vector parallel to the sample surface. This indicates that the surface state becomes a resonance far from the $\bar{\Gamma}$-symmetry point of the SBZ. However, the wave vector where the surface state becomes a resonance is not specified exactly, since there is no band calculation for bulk Bi, which describes the overall valence-band structures quantitatively as discussed above, and therefore the projection of the bulk electronic states on the SBZ is not specified. However, it is possible to conclude that at least this surface state at the wave vector of intersection becomes a resonance state. As shown in Fig. 5, it is also found that the dispersion of the surface resonance state, observed at a higher binding energy than the above surface state, is a rather complicated one, and is on the order of about 1.3 eV. The energy dispersion of this surface resonance state on clean Bi (111) is definitely determined in the present work for the first time. We believe that the rather complicated energy dispersion of this surface resonance state is due to hybridization with the bulk electronic states.

IV. CONCLUSION

We have performed an angle-resolved photoemission study of Bi (111). In the valence-band photoemission spectrum, we observed features derived from the Bi 6*p*-derived bulk valence band, a surface state in the spin-orbit gap, and a surface resonance state. From detailed angle-resolved photoemission spectra, the dispersion relations of the bulk valence bands of Bi were determined along the *T*-*U* high-symmetry line in the bulk BZ. From a comparison with the theoretical results of band calculations obtained by EPM and empirical TB method, it is found that both band calculations fail to quantitatively reproduce the present experimental results. However, the TB calculation seems to give results in better agreement with the experimental valence-band dispersion. In addition, the dispersion relation of the surface state in the spin-orbit gap and surface resonance state on Bi (111) were also determined experimentally along the $\bar{\Gamma}$-$\bar{M}$-symmetry line in the SBZ. From a comparison with the bulk experimental valence-band dispersion, it is found that the present surface state in a spin-orbit gap becomes a resonance at the finite wave vector parallel to the sample surface far from the $\bar{\Gamma}$-symmetry point of the SBZ.

ACKNOWLEDGMENTS

This work was supported by a Grant-in-Aid for Scientific Research from the Ministry of Education, Science, and Culture of Japan and a grant from the Core Research for Evolutional Science and Technology (CREST), Japan Science and Technology Corporation (JST).

[1] R. J. Needs, R. M. Martain, and O. H. Nielsen, Phys. Rev. B **33**, 3778 (1986).
[2] J.-P. Issi, Aust. J. Phys. **32**, 585 (1979).
[3] G. E. Smith, Phys. Rev. **115**, 1561 (1964).
[4] Y. H. Kao, Phys. Rev. **129**, 1122 (1963).
[5] R. D. Brown, R. L. Hartman, and S. H. Koenig, Phys. Rev. **172**, 598 (1968).
[6] V. S. Edel'man, Adv. Phys. **25**, 555 (1976).
[7] M. H. Cohen, Phys. Rev. **121**, 387 (1961).
[8] L. G. Ferreira, J. Phys. Chem. Solids **28**, 1891 (1967).
[9] L. G. Ferreira, J. Phys. Chem. Solids **29**, 357 (1968).
[10] S. Golin, Phys. Rev. **166**, 643 (1968).
[11] J. H. Xu, E. G. Wang, C. S. Ting, and W. P. Su, Phys. Rev. B **48**, 17 271 (1993).
[12] Y. Liu and R. E. Allen, Phys. Rev. B **52**, 1566 (1995).
[13] G. Jezequel, J. Thomas, and I. Pollini, Phys. Rev. B **56**, 6620 (1997).
[14] G. Jezequel, Y. Petroff, R. Pinchaux, and F. Yudurain, Phys. Rev. B **33**, 4352 (1986).
[15] F. Patthey, W.-D. Schneider, and H. Micklitz, Phys. Rev. B **49**, 11 293 (1994).
[16] A. Ishizaka and Y. Shiraki, J. Electrochem. Soc. **133**, 666 (1986).
[17] G. Jezequel, A. Barski, p. Steiner, F. Solal, P. Roubin, R. Pinchaux, and Y. Petroff, Phys. Rev. B **30**, 4833 (1984).
[18] P. J. Feibelman and D. E. Eastman, Phys. Rev. B **10**, 4932 (1974).
[19] T. Grandke, L. Ley, and M. Cardona, Solid State Commun. **23**, 897 (1977).